

Dynamic effects in fragmentation reactions

G.F. Bertsch^a and H. Esbensen^a

^a*Institute for Nuclear Theory, University of Washington, Seattle, WA 98195*

^b*Physics Division, Argonne National Laboratory, Argonne, IL 60439, USA*

Abstract

Fragmentation reactions offer a useful tool to study the spectroscopy of halo nuclei, but the large extent of the halo wave function makes the reaction theory more difficult. The simple reaction models based on the eikonal approximation for the nuclear interaction or first-order perturbation theory for the Coulomb interaction have systematic errors that we investigate here, comparing to the predictions of complete dynamical calculations. We find that stripping probabilities are underpredicted by the eikonal model, leading to extracted spectroscopic strengths that are too large. In contrast, the Coulomb excitation is overpredicted by the simple theory. We attribute this to a screening effect, as is well known in the Barkas effect on stopping powers. The errors decrease with beam energy as E_{beam}^{-1} , and are not significant at beam energies above 50 MeV/u. At lower beam energies, the effects should be taken into account when extracting quantitative spectroscopic strengths.

I. INTRODUCTION

Reactions of halo nuclei have given valuable spectroscopic information, often deduced with the help of simple reaction models such as the eikonal approximation [1–5] or first-order perturbation theory, see e.g. [6–12]. However, there are some situations where these models are not precise enough for the question under study. One such question is the

absolute spectroscopic factors associated with single-particle states in nuclei. Correlations reduce the spectroscopic factors from unity, but the precise reduction is not easily measured. While values close to one have been extracted from nuclear reaction experiments, electron scattering measurements yield reductions of several tens of percent. Other cases where accurate measurement are desired arise in the modeling of nuclear reactions in stars. A prominent example is the break-up cross section of ${}^8\text{B}$. The inverse process, the capture of protons on ${}^7\text{Be}$, has a crucial role in producing high energy neutrinos in the sun.

To assess the accuracy of the simple models, we have studied a Hamiltonian model that can be solved numerical to high precision, and compared with the predictions of the eikonal and the first-order perturbation theory. The Hamiltonian has the form of a three-particle problem: we consider as active coordinates the positions of the projectile, the target, and the halo nucleon. In the initial state, the nucleon is bound to a core to form the projectile ground state. The interactions absorb the nucleon or leave it in an excited state. To make the model tractable computationally, we assume that the projectile-target coordinate can be treated by classical dynamics. Then the problem reduces to a time-dependent one-particle dynamics, namely the evolution of the nucleon-core wave function in the external field of the target. This demands that the time-dependent Schrödinger equation be solved in a full three-dimensional representation of the nucleon-core wave function.

There are several computational methods available for solving the 3-D time-dependent Schrödinger equation, In some contexts a three-dimensional grid representation is very effective [13,14]. For the problem under study here, however, we find that a spherical representation with a radial mesh is most efficient. Centering the coordinate system on the center of mass of the projectile, the wave function can be accurately computed for the initial state. The arena in which the wave function evolves can also be large, because the radial mesh can easily extend to hundreds of femtometers. The spherical representation has been used by several groups previously, including ourselves [15] and others [16,17].

II. TECHNICAL DETAILS OF THE CALCULATIONS

We summarize here the model we use; a more detailed description can be found in ref. [18]. The only coordinates are the neutron's position with respect to the core, \mathbf{r} , and the projectile-target coordinate \mathbf{R} . For simplicity we assume a straight-line trajectory for the core-target motion, $\mathbf{R}(t) = \mathbf{b} + \mathbf{v}t$. This leaves the neutron-core and neutron-target potentials to be specified in the Hamiltonian. Again for simplicity we ignore spin-orbit interactions, taking the neutron-core potential U_{nc} to have a simple Woods-Saxon form, $U_{nc}(r) = -V_c f(\frac{r-R_c}{a_c})$, where $f(x) = (1 + e^x)^{-1}$. The initial state of the neutron $|0\rangle$ is an eigenstate of that potential. The neutron-target interaction is parameterized as a conventional optical potential $U_{nt}(r_{nt})$, which we have taken from the parameterization in Ref. [19]. The core-target nuclear interaction is set to zero for convenience.

The immediate object of the reaction calculation is the neutron wave function in the final state. In the eikonal approximation, valid when the target interaction has a very short duration, the final state wave is obtained by a simple multiplicative factor. In the present model, this is

$$\Psi_f(\mathbf{r}) = S_{nt}(|\mathbf{b} - \alpha\mathbf{r}_\perp|) |0\rangle = \exp\left(\int_{-\infty}^{\infty} \frac{dz}{i\hbar v} U_{nt}(\sqrt{|\mathbf{b} - \alpha\mathbf{r}_\perp|^2 + z^2})\right) |0\rangle, \quad (1)$$

where $|0\rangle$ is the initial ground state wave function, v is the projectile velocity, and $\alpha = (A - 1)/A$, in terms of the projectile mass number A .

For the dynamic calculation we integrate the time-dependent Schrödinger equation over a finite time interval $-T < t < T$, where $t = 0$ at closest approach and T is chosen large enough to cover the duration of the interaction with the target. The strictly numerical parameters associate with the wave function are radial mesh spacing Δr , the radius of the spherical arena r_{max} , and the cutoff angular momentum l_{max} in the spherical representation.

We also need to specify the algorithm for the time integration and its time step Δt . We use a time propagator that is unitary with respect to the nucleon-core Hamiltonian, namely the well-known finite difference expression [20],

$$\exp(-iH\Delta t) \approx \frac{1 - iH\Delta t/2}{1 + iH\Delta t/2}. \quad (2)$$

The neutron-target potential is included by a simple first-order integration, adding $-iU_{nt}\Delta t$ to the denominator of eq. (2.2). We also use a variable time step that is longer when the projectile is far from the target. This is done by the transformation of the time variable t to variable w , [21]

$$t = \frac{1}{v} \left(\sqrt{(D/2)^2 + b^2} \sinh(w) + (D/2)w \right),$$

and taking a uniform step in w . In this equation, b is the impact parameter, v is the beam velocity, and D is the distance of closed approach in a head-on collision. We have chosen the radial step $\Delta r = 0.2$ fm, and a sphere radius r_{max} between 50 and 200 fm. To calculate breakup probabilities, it is sufficient to use $r_{max} = 50$ fm but to get realistic momentum distributions one needs a larger radius. The integration is started with the projectile-target y separation specified at some value $y_0 = -vT$, and the time integration is performed up to a time $+T$. When there is no Coulomb interaction, it is sufficient to take $-40 < y < 40$ fm. If Coulomb interactions are present, the integration should include distances going well beyond the adiabatic cutoff distance, given by v/ω , where ω is the smallest excitation energy in the halo nucleus. In practice, this requires extending the distance to a few hundred fm.

Concerning the decomposition into l and m , we find that it is adequate to limit the channels to $l \leq l_{max} = 12$. For the s -wave halo orbital, the number of (lm) channels is 91 taking the scattering plane symmetry into account. This is about the most we are able to handle within a reasonable computation time. For consistency, we include all contributing terms in the multipole expansion of U_{nt} .

III. OBSERVABLES

All physical quantities are computed from the final state halo wave function, $\Psi_f(\mathbf{r}) = \Psi(\mathbf{r}, T)$. The most important observables among the angle-integrated cross sections are the neutron removal probability P_{-1n} , the stripping probability P_{Str} , and the diffractive

dissociation probability P_{Diff} . These are defined

$$P_{-1n} = P_{\text{Str}} + P_{\text{Diff}}$$

where

$$P_{\text{Str}}(b) = 1 - \langle \Psi_f | \Psi_f \rangle,$$

$$P_{\text{Diff}}(b) = \langle \Psi_f | \Psi_f \rangle - \sum_n |\langle n | \Psi_f \rangle|^2, \quad (3)$$

and where n sums over bound states of the halo nucleon in the projectile. Besides the integrated diffraction probability, differential probability distributions in the final state are measured and provide important information. To compute momentum distributions, we project the final state wave function onto scattering states of the nucleon-core Hamiltonian.

We define amplitudes S_{klm} so that the wave function in momentum space is

$$\Psi_f(\mathbf{k}) = \frac{1}{k} \sum_{lm} Y_{lm}(\hat{k}) S_{klm}(b). \quad (4)$$

Thus the complete final state momentum distribution will be given by

$$\frac{d^3 P(b, \mathbf{k})}{d\vec{k}} = |\Psi_f(\mathbf{k})|^2 = \frac{1}{k^2} \left| \sum_{lm} Y_{lm}(\hat{k}) S_{klm}(b) \right|^2. \quad (5)$$

The amplitudes S_{klm} are calculated as overlaps of the final state wave function with the scattering states $|klm\rangle = \frac{1}{r} \phi_{kl}(r) Y_{lm}(\hat{r})$. Two components of the momentum distribution are particularly interesting, namely, the angle-averaged distribution and the longitudinal momentum distribution. The angle-integrated distribution, which we define as

$$\frac{dP(b, k)}{dk} = \sum_{lm} |S_{klm}(b)|^2, \quad (6)$$

is closely related to the decay-energy spectrum. As will be seen, it can reveal the location of unbound single-particle resonances in the projectile. The longitudinal momentum distribution provides information about the reaction dynamics, particularly related to the time duration of the collision. It is given by

$$\frac{dP(k_z)}{dk_z} = 2\pi \int_{|k_z|}^{\infty} \frac{dk}{k} \sum_m \left| \sum_{l \geq |m|} Y_{lm}(\theta_k) \tilde{S}_{klm} \right|^2, \quad (7)$$

where θ_k is defined $\cos \theta_k = k_z/k$ and the tilde on S_{klm} indicates that the angular momentum expansion is done in a coordinate system with the z -axis along the beam direction.

IV. NEUTRON HALOS

The example of ^{11}Be , a typical neutron halo nucleus, is discussed in ref. [18]. Here the halo neutron is in an s-orbital bound by $E_b = 0.5$ MeV. Comparing the eikonal and the dynamic calculations on the target ^{12}C , we found that the eikonal reproduces the b -dependence of the probabilities quite well, but underestimates them by an amount that depends largely on the beam energy. The underprediction of the stripping is easy to understand qualitatively. In the eikonal approximation, the absorptive potential of the target acts only on the halo density in the immediate path. In the full dynamics, there is also a probability flux from the halo wave function into the target region in response to earlier absorption and diffraction. More quantitatively, one would expect from perturbation theory that the eikonal would to converge to the full dynamics as

$$1/v \sim E_{beam}^{-1/2}$$

for real potentials and

$$1/v^2 \sim 1/E_{beam} \tag{8}$$

for absorptive potentials. Both the stripping and diffraction probabilities follow the dependence of eq. (4.1) above $E_{beam} = 20$ MeV/nucleon. Our numerical results are well fit by the parameterization

$$P_{eik}/P_{dyn} = 1 - C/E_{beam}$$

with $C \approx 4.5$ MeV.

Even if the probabilities are calculated to high accuracy, it is still difficult to determined absolute spectroscopic strengths due to necessity to integrate over impact parameter with a model of the core-target absorption. A less ambitious use of reaction theory is to apply it only to relative spectroscopic strengths of different single-particle states. In ref. [18] we also compared extracted spectroscopic strengths for different shell orbitals, finding that the eikonal is an excellent approximation when used this way. For example, at a beam energy

of 40 MeV/nucleon, the difference in the probability ratios is only a few percent over the range of bound state angular momenta from 0 to 2 and binding energies of 0.5 to 3.0 MeV.

A. Momentum distributions

As mentioned earlier, the energy distribution of the nucleon with respect to the core provides information about the single-particle resonances. The distribution in ^{11}Be is shown in Fig. 7 of ref. [18]. One sees a broad peak at about 80 MeV/c and superimposed a very narrow peak at 55 MeV/c, corresponding to a resonance energy of 1.8 MeV. The shape of the distribution is very well described by the eikonal model. The narrow peak is due to a d -wave resonance of the projectile potential. This resonance is seen experimentally, but at a somewhat lower energy. It should be noted that models which neglect the final state core-particle interaction (e.g. the transfer-to-continuum model [22]) will miss resonance peaks such as found here. The broad peak is rather insensitive to beam energy and the details of the target interaction.

We next turn to the longitudinal momentum distribution, which is interesting from several perspectives. Of all the momentum distributions, it is least sensitive to the details of the neutron-target interaction. In fact, to some approximation it just reflects the longitudinal momentum content of the initial bound state. However, one feature of the longitudinal momentum distribution, its asymmetry in the projectile frame, is due to the finite duration of the collision and is completely beyond the scope of the eikonal approximation. This is seen in Fig. 7 of ref. [18] for the diffractive breakup of ^{11}Be . The distribution obtained from the dynamic calculation is 10% broader than the eikonal predicts. It also has a pronounced tail going to lower momenta with respect to the target, an effect that is entirely absent from the eikonal result. The low-energy wing of the distribution can be attributed to processes whereby the target drags the neutron down to a low-momentum state in its frame. This process was first described with the time-dependent calculations of ref. [14]. We have also discussed it in more detail in our ref. [18].

V. PROTON HALOS

We now turn to proton halos, taking as a test case the nucleus ^{17}F , whose last proton is a $d_{5/2}$ orbital bound by 0.6 MeV. To reproduce the experimental energies for the two bound states in ^{17}F , different potential radii are used for the d - and the other partial waves in U_{nc} . The diffuseness and well depth are taken as $a = 0.67$ fm and $V = -54.477$ MeV in all cases. For the d -wave, the radius is taken as $R_s = 3.242$ fm, which fits the separation energy $S_p=0.6$ MeV of the $5/2^+$ ground state of ^{17}F . For the s -wave and all other partial waves, the radius is taken as $R_s = 3.074$ fm. This reproduces the separation energy of 0.1 MeV of the $1/2^+$ excited state. This simplified Hamiltonian reproduces the measured radiative capture cross section [23] to the ground of ^{17}F fairly well. The capture rate to the $1/2^+$ state is somewhat exaggerated at higher energies, roughly by 30% at 2–3 MeV. The nuclear interactions are treated the same as before. The Coulomb interaction with the target is represented by the non-relativistic E0, E1, and E2 multipole fields, with the full radial dependence (i.e., not making the usual far-field approximation).

The results of dynamical calculations are compared to the eikonal approximation for the nuclear induced breakup, and to first-order perturbation theory for Coulomb dissociation. The eikonal calculation is performed for a straight-line trajectory at an effective impact parameter equal to the minimum distance on the Coulomb trajectory, $b_{eff} = D/2 + \sqrt{b^2 + (D/2)^2}$, where b is the actual impact parameter and $D = ZZ_T e^2/E_{cm}$. The first-order Coulomb dissociation, on the other hand, is calculated on a Coulomb trajectory, using the non-relativistic far-field form factors. The results for the diffractive breakup at 10 MeV/n beam energy on a ^{208}Pb target are shown in Fig. 1. The squares show the results of the dynamic calculation without any significant approximation. The first-order perturbation theory with the far-field Coulomb interaction is shown as a dashed line. Here we have included only E1 and E2 multipoles in the Coulomb field; higher multipoles give negligible contribution. One sees that the first-order Coulomb overestimates the probability. The dynamic effect thus goes in opposite direction for the Coulomb and the nuclear inter-

action. This is very plausible; the interactions have opposite signs and one might expect a screening effect with the Coulomb, which seems to be observed. However, the physics is actually more subtle as we will see in the next section. At small impact parameter, the nuclear interaction is significant and its antiscreening effect counterbalances the Coulomb screening. We also compare with the eikonal model of the nuclear interaction, shown as the solid line.

VI. THE BARKAS EFFECT

The dynamic polarization from the Coulomb field is well-known in atomic stopping theory. It was first recognized by Barkas et al. [24] in measurements of the range of π^+ and π^- . Although the pions were produced in emulsion under identical conditions (with the same kinetic energy), it was found the range was larger for π^- than for π^+ . The effect is therefore referred to as the Barkas effect - or the Z^3 -effect - for reasons that are discussed below. The Barkas effect was later confirmed in stopping power measurements, as for example, of protons and anti-protons [25], with anti-protons having the smaller stopping power. In the Coulomb dissociation of a proton-halo nucleus, the dynamic polarization effect is expected to lead to a reduction of the dissociation probabilities compared to first-order perturbation theory. This expectation is based on the analogy with the reduced stopping powers of π^- and anti-protons, where the Coulomb forces on the electrons in a solid are repulsive, just as they are in the case of the Coulomb dissociation of a proton-halo nucleus.

However, at a quantitative level the effect is far from trivial to understand. It may be analyzed in second-order perturbation theory [26], expanding the amplitude for a dipole transition as

$$a_{E1} = a_{E1}^{(1)} + a_{E1,E2}^{(2)} + \dots \quad (9)$$

Here $a_{E1}^{(1)}$ is the first-order amplitude, and the second-order amplitude consists of a dipole followed by a quadrupole transition, and vice versa. The resulting dipole excitation probability is

$$P_{E1} \approx |a_{E1}^{(1)}|^2 + 2 \operatorname{Re}[a_{E1}^{(1)*} a_{E1,E2}^{(2)}] + \dots \quad (10)$$

The second term is of order Z^3 in the charge Ze of the penetrating particle, and it has been used to account for the atomic Barkas effect [25,27,28], or Z^3 -effect. In the Coulomb dissociation of ^{17}F one should also consider the effect on quadrupole transitions. The second-order transitions would then consist of two successive dipole transitions, or two successive quadrupole transitions. Note that the Z^3 correction would vanish if the external quadrupole field is neglected.

Naively, inside the adiabatic cutoff distance the dipole and quadrupole amplitudes depend on target charge, beam velocity and impact parameter as

$$a_{E1} \sim \frac{Z}{bv}$$

and

$$a_{E2} \sim \frac{Z}{b^2v}.$$

Then the second-order probability from eq. (6.2) varies as

$$\frac{Z^3}{b^4v^3}. \quad (11)$$

However, there are two terms in the second-order amplitude corresponding to the two time orderings of the E1 and E2, and these tend to cancel. In fact, in the absence of any binding potential, the excitation is by the recoil in elastic Coulomb scattering, for which the Z^3 and higher order terms cancel exactly. When the calculation is carried for the harmonic oscillator model, there is found to be a partial cancelation, giving a net dependence as

$$\frac{Z^3}{b^2v^5}, \quad (12)$$

falling off much more rapidly with beam velocity than eq. (6.3).

When we analyze the diffractive dissociation of the proton halo, we find a dependence on beam energy that is intermediate between eq. (6.3) and (6.4). In order to separate the Barkas Z^3 effect from other approximations, we repeated the dynamical calculation with the

opposite sign of the Coulomb form factors. The resulting Coulomb dissociation probability is denoted by $P_{\text{CD}}^{(\pm)}(b)$. Let us write the probability for the two signs as

$$P_{\text{CD}}^{(\pm)}(b) = P_{\text{CD}}^{(1)}(b) A [1 \pm B], \quad (13)$$

where $P_{\text{CD}}^{(1)}(b)$ is the first-order probability for distant collisions, A is a Z -even correction factor given by

$$A = \frac{P_{\text{CD}}^{(+)} + P_{\text{CD}}^{(-)}}{2P_{\text{CD}}^{(1)}}, \quad (14)$$

and

$$B = \frac{P_{\text{CD}}^{(+)} - P_{\text{CD}}^{(-)}}{P_{\text{CD}}^{(+)} + P_{\text{CD}}^{(-)}} \quad (15)$$

is the Barkas factor. We found that that A is close to one except at the lowest beam energy and smallest impact parameters. In contrast, B is significant at all beam energies and impact parameters. The correction factor B corresponding to the $P_{\text{CD}}^{(\pm)}$ for a ^{208}Pb target is shown in Fig. 2.

Here we will propose an empirical parameterization of the Barkas factor B based on the above numerical findings. We have also calculated the B factor for a ^{58}Ni target, verifying that the target charge-dependence is well fit by Z^3 . However, the beam-energy dependence is weaker than the $E_{\text{beam}}^{-3/2}$ power given by Eq. (6.4). In fact, it is closer to a simple inverse dependence, as we found earlier for the dynamic effects on the nuclear breakup [18].

The impact parameter dependence of the B factor is quite mild. We can parameterize it by the functional form $(b^2 + a^2)^{-1/2}$, where a is an adjustable cutoff distance. We thus adopt the parameterization

$$B(b, E_{\text{beam}}) = C \frac{Z_{\text{T}} e^2}{E_{\text{beam}}} \frac{1}{\sqrt{b_{\text{eff}}^2 + a^2}}, \quad (16)$$

where b_{eff} is the minimum projectile-target distance of a Coulomb trajectory. We found a fair fit to all the conditions except the 10 MeV/nucleon collisions with a parameterization $C = -1.68$, and $a = 20$ fm in Eq. (6.8). This indicates that other higher-order processes

become important at 10 MeV/u, consistent with the fact that the Z -even factor A also becomes larger than one at this energy.

We thus have come to a good qualitative understanding of the Barkas effect in the Coulomb dissociation of proton-halo nuclei. It is the most dominant higher-order process at higher beam energies, large impact parameters, and for low- Z targets. At low beam energies and for high- Z targets, other higher order processes become important. This is evidenced by the fact that the simple Z_T -scaling of the Barkas factor (6.8) breaks down and also that the Z -even factor A becomes larger than one.

ACKNOWLEDGMENTS

This work was supported by the U. S. Department of Energy, Nuclear Physics Division, under Contract W-31-109-ENG-38, and Grant DE-FG03-00ER-41132.

REFERENCES

- [1] G. Bertsch, H. Esbensen, and A. Sustich, *Phys. Rev. C* **42**, 758 (1990).
- [2] Y. Ogawa, K. Yabana, and Y. Suzuki, *Nucl. Phys. A* **543**, 722 (1992).
- [3] J. S. Al-Khalili, J. A. Tostevin, and I. J. Thompson, *Phys. Rev. C* **54**, 1843 (1996).
- [4] K. Hencken, G. F. Bertsch, and H. Esbensen, *Phys. Rev. C* **54**, 3043 (1996).
- [5] J.A. Tostevin, *J. Phys. G* **25**, 735 (1999).
- [6] C.A. Bertulani and G. Baur, *Phys. Rep.* 163 299 (1988).
- [7] D. Sackett, et al., *Phys. Rev. C* **48** 118 (1993).
- [8] Y. Iwata, et al., *Phys. Rev. C* **62** 064311 (2000).
- [9] T. Motobayashi *et al.*, *Phys. Rev. Lett.* **73** (1994) 2680.
- [10] T. Kikuchi *et al.*, *Eur. Phys. J. A* **3** (1998) 213.
- [11] N. Iwasa *et al.*, *Phys. Rev. Lett.* **83** (1999) 2910.
- [12] B. Davids *et al.*, *Phys. Rev. Lett.* **86** (2001) 2750; *Phys. Rev. C* **63**, 065806 (2001).
- [13] D. Lacroix, J. Scarpaci, and Ph. Chomaz, *Nucl. Phys. A* **658**, 273 (1999).
- [14] M. Fallot, J. A. Scarpaci, D. Lacroix, Ph. Chomaz, and J. Margueron, arXiv preprint nucl-th/0101011.
- [15] H. Esbensen, G. F. Bertsch, and C. A. Bertulani, *Nucl. Phys. A* **581** (1995) 107.
- [16] V. S. Melezhik and D. Baye, *Phys. Rev. C* **59** (1999) 3232.
- [17] T. Kido, K. Yabana, and Y. Suzuki, *Phys. Rev. C* **53** (1996) 2296.
- [18] H. Esbensen and G. F. Bertsch, *Phys. Rev. C* **64**, 014608 (2001).
- [19] R. L. Varner, W. J. Thompson, T. L. McAbee, E. J. Ludwig, and T. B. Clegg, *Phys.*

Rep. 201, 57 (1991).

- [20] W. H. Press, et al., *Numerical Recipes in C*, (Cambridge University Press, New York, 1986), eq. 17.2.33.
- [21] K. Alder and A. Winther, *Electromagnetic Excitation* (North-Holland, Amsterdam 1975).
- [22] A. Bonaccorso and F. Carstoiu, *Phys. Rev. C* 61, 034605 (2000), and references therein.
- [23] R. Morlock *et al.*, *Phys. Rev. Lett.* 79 (1997) 3837.
- [24] W. H. Barkas, N. J. Dyer, and H. H. Heckman, *Phys. Rev. Lett.* 11 (1963) 26.
- [25] L. H. Andersen *et al.*, *Phys. Rev. Lett.* 62 (1989) 1731.
- [26] K. W. Hill and E. Merzbacher, *Phys. Rev. A* 5 (1974) 156.
- [27] J. C. Ashley, R. H. Ritchie, and W. Brandt, *Phys. Rev. B* 5 (1972) 2393; *Phys. Rev. A* 8 (1973) 2402.
- [28] J. D. Jackson and R. L. McCarthy, *Phys. Rev. B* 6 (1972) 4131.
- [29] H. Esbensen and G. F. Bertsch, *Nucl. Phys. A* 600, 37 (1996).

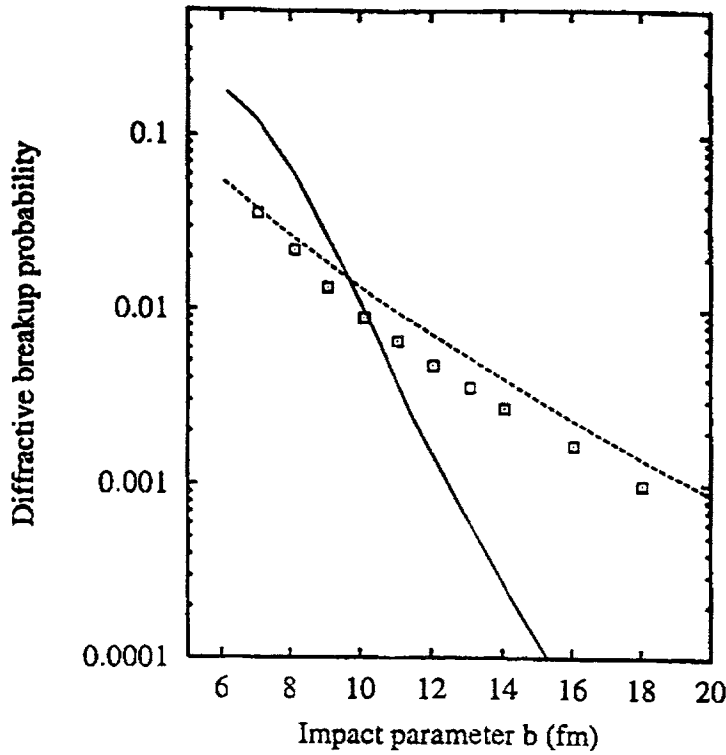


Fig. 1. Diffractive breakup probability for ^{17}F scattering on a ^{208}Pb target at 10 MeV/nucleon. Dashed line is the first-order Coulomb theory, and solid line is the nuclear eikonal theory. The full dynamic calculation is shown by the squares.

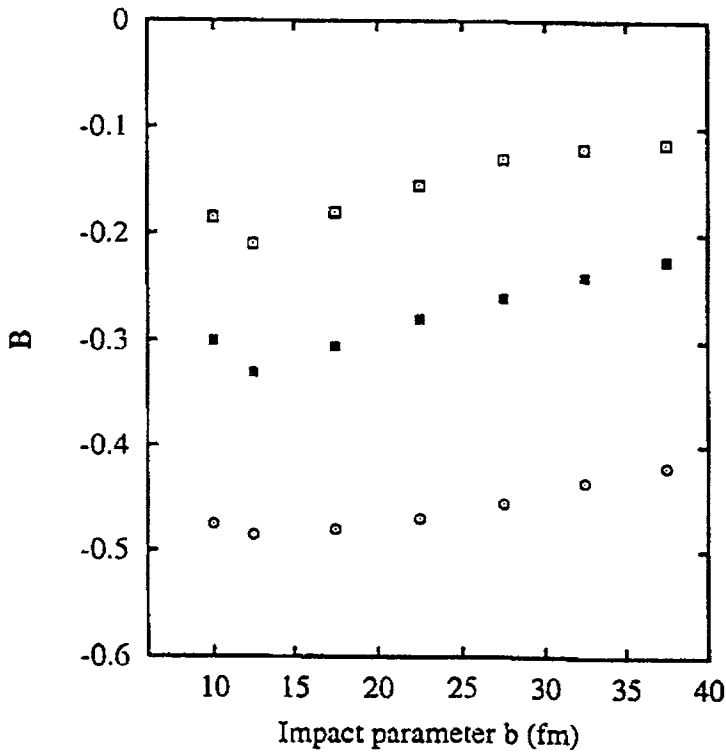


Fig. 2. Barkas B factor for ^{17}F scattering on a ^{208}Pb target at 10, 20 and 40 MeV/nucleon, shown by the open squares, filled squares, and circles, respectively.